Composites Science and Technology, Volume 72, Issue 7, 13 April 2012, Pages 799-805

Modelling flow and filtration in liquid composite moulding of nanoparticle loaded thermosets

Elisabete F. Reia da Costa*, Alexandros A. Skordos

Cranfield University, Composites Centre, MK43 0AL, UK

tel: + 44 (0) 1234 750 111; fax: + 44 (0) 1234 750 875

*Corresponding author's email: e.f.r.costa@cranfield.ac.uk

Abstract

This paper presents analytical and numerical models of liquid moulding of hybrid composites. An 1-D analytical solution of Darcy's problem, accompanied by nanoparticle filtration kinetics and conservation, has been developed. A non-linear finite difference model incorporating variations in permeability, porosity and viscosity as a function of local nanoparticle loading was formulated. Comparison of the two models allowed verification of their validity, whilst a mesh sensitivity study demonstrated the convergence of the numerical scheme. The limits of validity of the analytical solution were established over a range of infiltration lengths and filtration rates for different nanoparticle loadings. The analytical model provides an accurate and efficient approximation of through thickness infusion of hybrid composites, whereas use of the numerical scheme is necessary for accurate simulation of in-plane filling processes. The models developed here can serve as the basis of process design/optimisation for the production of hybrid composites with controlled distribution of nano-reinforcement.

Keywords

A. Nano particles, A. Hybrid composites, C. Modelling, E. Resin transfer moulding (RTM)

1. Introduction

The incorporation of carbon nanoparticles in fibre reinforced composites has become a matter of great interest in the aerospace industry in recent years. The extraordinary electrical, thermal and mechanical properties of carbon nanoparticles combined with the structural and properties of lightweight fibrous composites makes hybrid composites an attractive class of materials. Liquid moulding techniques such as resin transfer moulding (RTM) and vacuum assisted resin transfer moulding (VARTM) are common techniques for the manufacture of fibre reinforced composites. When carbon nanoparticle filled resins are utilised in liquid moulding processes, a stable and homogenous dispersion of the nanoparticles in suspension is paramount for an efficient transfer of their unique properties to the final composite [1, 2]. Increasingly higher nanoparticle contents lead to unacceptably high viscosity suspensions for infusion. In addition to the viscosity issues related to high particle content, filtration of particles by the reinforcement can also slow down the resin flow front and lead to long infusion cycles or ultimately to incomplete filling. Particle filtration is a complex phenomenon, which depends on a combination of processing conditions, such as the injection pressure or flow rate and flow direction; as well as the material properties, namely chemical and physical characteristics of the particles, the resin and the porous media. Cake filtration and deep bed filtration are the two main mechanisms occurring during liquid moulding of carbon nanoparticle filled resins. Cake filtration is manifested as volume capture taking place when the particle size is larger than the pore size. Deep bed filtration is characterised by the gradual capture of particles smaller than the pore channels. Continuous capture of particles leads to narrowing of the available pore channels which may ultimately result in cake filtration. Particle size governs the distinct volume and/or

surface phenomena taking place during deep bed filtration [3]. Generally, for suspensions containing large particles ($d \geq 30$ μm) volume phenomena prevail over surface phenomena; whilst for small particles ($d \sim 1$ μm) surface interactions are predominant; for particle dimensions between 3 μm and 30 μm, both volume and surface phenomena can occur. Other classifications of the filtration mechanisms are based on the ratio between the particle mean diameter and the grain mean diameter of a grain bed [4, 5].

In composites processing the objective may be to entrap all the particles in one layer, or achieve an uniform distribution of particles in the composite, or even create a particle concentration gradient characterised by high carbon nanoparticle content in some regions critical to the design/functionality of the component and low content regions in the rest of the part. In all of this potential scenaria a good understanding of the infusion process and the main effects filtration has on process parameters such as viscosity, porosity and permeability is paramount for process design and control.

Deep bed filtration phenomena through porous media have been widely studied in several natural and industrial fields/areas, such as oil extraction, wastewater treatment and contaminated ground water flow [6-8]. The modelling of flow of particle filled resins in fibrous media in the manufacture of hybrid composites by liquid moulding has received limited attention up to date. A 2-D Eulerian multiphase approach combined with a control volume finite element model has been used in order to predict the trajectories of spherical carbon nanoparticles in a resin suspension during liquid moulding [9, 10]. A 2-D numerical model coupling Stokes-Brinkman laws, accounting for hydrodynamic interactions between the particles and the fibre walls, was utilised to describe the flow in dual-scale porous media during liquid composite moulding [11].

Particle filtration mechanisms were investigated by Nordlund et al. [12] in a resin infusion scenario by velocimetry and microscopy. A stochastic approach, based on the Monte Carlo method has been proposed to simulate liquid filtration of spherical particles through non-woven fibrous media [13]. Macroscopic models of filtration such as the ones developed by Erdal et al. [14] and subsequently enhanced by Lefevre et al. [15, 16] couple Darcy's flow with a conservation of mass and filtration kinetics. This type of approach was used in combination with probabilistic methods to determine the particle concentration distribution in the thickness direction of a composite manufactured during VARTM infusion [17]. Recently, a constitutive model approach for filtration was developed in [18], while the filtration constant was determined experimentally as a function of the suspension concentration and the shear rate. Despite the contribution of this experimental methodology, the experimental results did not validate the model.

In the present work an analytical solution for the linear flow of carbon nanoparticle filled resins during liquid moulding of composites is derived. The solution for the concentration of suspended and filtered particles is obtained by coupling Darcy's law with mass conservation and filtration kinetics. In addition a finite difference filling simulation methodology accounting for porosity, permeability and viscosity variations in time and position is implemented for the non-linear case. The two models are compared and the convergence of the numerical model is investigated. The limits of validity of the linear approximation associated with the analytical solution are explored over a wide range of processing conditions.

2. Model development

2.1. Boundary value problem

The physics of the one-dimensional flow and filtration problem are represented by conventional Darcy's law (Eq.2) associated with a continuity condition (Eq.1) and a particle mass conservation (Eq.3) combined with filtration kinetics (Eq.4) based on work by Lefevre et al. [15, 16]. The suspension Darcy velocity U is driven by the pressure P gradient in the cavity, and is proportional to the permeability over viscosity ratio K/η. The mass balance represented by Eq.3 accounts for the amount of particles entering and exiting the domain, which corresponds to the total flux of retained and suspended particles, where C and σ represent the concentration of suspended and retained particles, respectively. The concentration time derivative of retained $\partial\sigma/\partial t$ and suspended particles $\partial\varepsilon C/\partial t$, together with the flux of suspended particles along the reinforcement length $U\,\partial C/\partial x$ contribute to the total balance of particles in the composite at each time step and position. The latter equation neglects both particle diffusion and sedimentation. A constitutive law (Eq.4) describes the kinetics of retention and possible re-suspension of particles. The first term of Eq.4 corresponds to the retention of particles which is proportional to the flux of suspended particles UC. The proportionality constant k_o is called the filtration constant. Any dependence of the filtration constant on the concentration of retained particles was assumed negligible. The second term in the RHS of Eq. 4 represents the rate of particle re-suspension. The latter is considered to be proportional to the product of the concentration of retained particles by the flux of suspended particles and k_r represents the re-suspension constant. The problem described by Eqs (1)-(4) has four unknowns: the velocity (U), the pressure (P) and the concentration of suspended (C) and retained (σ) particles.

$$\frac{\partial U}{\partial x} = 0 \qquad (1)$$

$$U = -\frac{K}{\eta}\frac{\partial P}{\partial x} \tag{2}$$

$$\frac{\partial(\sigma + \varepsilon C)}{\partial t} + U\frac{\partial C}{\partial x} = 0 \tag{3}$$

$$\frac{\partial \sigma}{\partial t} = k_0 UC - k_r \sigma UC \tag{4}$$

A schematic of the 1-D flow and filtration problem is shown in Fig. 1. The resin flow front position (h) is considered equal to zero at the beginning of the filling process. Throughout the injection period, the concentration of suspended particles at the inlet equals the initial concentration of particles in the resin C_0, whilst the retention of particles at the resin flow front position is considered to be equal to zero. The pressure at the flow front position is equal to the vacuum pressure P_∞. Particle re-suspension is considered negligible ($k_r = 0$) since the flow direction is constant during injection.

The boundary condition of the flow problem at the inlet of the flow can be of the first type (Dirichlet), the second type (Neumann) or a combination of the two depending on the control strategy implemented in production. When considering a pressure controlled injection, the pressure at the inlet position corresponds to the injection pressure P_o. In the case of flow control the resin flow at the inlet V_o is kept constant throughout the process. In the case of flow control with a maximum pressure constraint, which is the most realistic condition for an industrial setup, the resin flow is constant at V_o up to the time t_o at which the pressure required to sustain the constant flow exceeds a certain pressure limit P_o. This type of boundary condition is implemented as a complementarity problem. Eqs.5-6 summarise this set of boundary conditions.

$$h(0) = 0,\ C(0, t) = C_0,\ \sigma(h(t), t) = 0,\ P(h(t), t) = P_\infty \tag{5}$$

$$P(0, t) = P_o \tag{6.a}$$

$U(0, t) = \varepsilon V_o$ (6.b)

$(P(0,t)-P_o)\,(U(0,t)-\varepsilon V_o)=0,\ P(0,t)-P_o<0,\ U(0,t)-\varepsilon V_o<0$ (6.c)

where Eq.6.a corresponds to a prescribed pressure condition at the inlet, Eq.6.b to prescribed flow and Eq.6.c to prescribed flow subject to a pressure constraint.

2.2. Analytical solution of the linear problem

The solution for the concentration of suspended C and retained particles σ presented in Eqs.7 and 8 is independent of the inlet flow boundary condition type (Eq.6) and is determined via combination of Eq.3 and 4 and considering the linear assumptions of constant permeability, viscosity and porosity; zero re-suspension of particles; and retention rate proportional to the flux of particles.

$$C = C_o \exp(-k_o x) \tag{7}$$

$$\sigma(x,t) = \varepsilon k_o C_o \exp(-k_o x)\ [h(t) - x] \tag{8}$$

Term $h(t)$ refers to the flow front evolution which depends on the inlet boundary condition. Under linearity the concentration of suspended particles is dependent only on position as a consequence of the assumptions of zero re-suspension and proportionality of retention rate to the flux of particles. In contrast, the concentration of retained particles is time dependent due to the cumulative character of filtration.

The total concentration of suspended and retained nanoparticles over the volume of liquid (T) is obtained by combining Eqs.7-8 with the solutions of the linear free boundary 1-D Darcy's. The solution for the case of prescribed pressure at the inlet (Eq.6.a) is:

$$T(x,t) = C_o e^{-k_o x}\left[1 + \varepsilon k_o\left(\sqrt{\frac{2K}{\varepsilon\eta}(P_o - P_\infty)\,t} - x\right)\right] \tag{9}$$

In the case of prescribed flow at the inlet (Eq.6.b) the boundary value problem yields

$$T(x,t) = C_o e^{-k_o x}\left[1 + k_o\left(V_o t - \varepsilon x\right)\right] \tag{10}$$

In the case of the combined boundary condition expressed by Eq.6.c the solution is:

$$T(x,t) = \begin{cases} C_o e^{-k_o x}\left[1 + k_o\left(V_o t - \varepsilon x\right)\right], & t \le \dfrac{\varepsilon K}{V_o^{\,2}\eta}\left(P_o - P_\infty\right) \\ C_o e^{-k_o x}\left[1 + \varepsilon k_o\left(\sqrt{\dfrac{2K\ t}{\varepsilon\eta}\left(P_o - P_\infty\right) - \left(\dfrac{K}{\eta V_o}\right)^2\left(P_o - P_\infty\right)^2} - x\right)\right], & t > \dfrac{\varepsilon K}{V_o^{\,2}\eta}\left(P_o - P_\infty\right) \end{cases} \tag{11}$$

These solutions reproduce the expected limit behaviour with respect to the value of k_o, i.e. a total loading equal to the initial suspended concentration (C_o) for zero filtration constant and loading equal to zero everywhere except the inlet in the case of infinite filtration.

2.3. Non-linear material models

Filtration of carbon nanoparticles by the reinforcement results in variations in material properties. These variations need to be addressed for an accurate prediction of the flow solution, when some of the linearity assumptions break down.

The narrowing of the reinforcement flow channels caused by the accumulation of nanoparticles results in a reduction of porosity as the resin flow front progresses. The contribution of resin entrapped within particle aggregates or between particles and reinforcement was neglected due to the diluted nature of the suspension and limited particle retention. The following relation is adopted to account for this effect:

$$\varepsilon(x,t) = \varepsilon_o - \frac{\sigma\left(x,t\right)}{\rho_{NP}} \tag{12}$$

where ε_o denotes initial porosity and ρ_{NP} the density of the nanoparticles. It should be noted that in the conditions used in this work the influence on porosity is negligible due to the small particle retention concentration compared to the volume fraction of the liquid. However, Eq.12 allows application of the model in situation of high retention.

The Kozeny-Carman relation can be used to describe the dependence of permeability on porosity [19, 20] as follows:

$$K(x,t) = A\frac{\varepsilon(x,t)^3}{\left(1-\varepsilon(x,t)\right)^2} \tag{13}$$

where A represents a constant. Similarly to the porosity case, Eq.13 was only adopted to allow generalisation of the model since the influence of retention on permeability is expected to be weak in the conditions of this study. The implementation of the model presented here is consistent with other permeability sub-models available in the literature.

Variations in suspended particle concentration lead to variations in viscosity. The model presented in [21] was adopted here to represent this effect as follows:

$$\eta(x,t) = \eta_o\left(1-\frac{C(x,t)}{\varphi_m\rho_{NP}}\right)^{-\eta_I\varphi_m} \tag{14}$$

Here η_o denotes the viscosity of the liquid medium, φ_m is the packing fraction of the filler and η_I is the intrinsic viscosity of the filler which expresses the sensitivity of the suspension viscosity to the filler volume fraction at the limit of negligible filler content. The selection of this material sub-model to express the dependence of viscosity on nanoparticle content is based on the successful representation of this non-linear dependence by Eq.14 as well as the incorporation of a physically meaningful parameter (packing fraction) that controls the high concentration behaviour without the need of demanding experimental effort.

2.4. Finite difference formulation and implementation

A 1-D finite difference model accounting for the material nonlinear behaviour was developed. The formulation is suitable for the simulation of both 1-D in-plane flow in

an RTM scenario and through the thickness flow in infusion. It should be noted that the implementation also allows for the incorporation of a generic filtration kinetics equation instead of Eq.4. However, the type of kinetics presented in Eq.4 is used here, whilst all the results presented concern the case of zero re-suspension coefficient.

The finite difference implementation uses a uniform grid representation of the domain of total length L comprising N grid points x_i.

The time discretisation is non uniform and allows a convenient treatment of the one dimensional free boundary problem by selecting a time step that matches the movement of the flow front from its current position to the next grid point t^j. The total number of time increments is not known a priori since it depends on the length of the modelling domain and the evolution of velocity during the solution.

Due to the 1-D character of the problem Darcy velocity does not vary in space but only in time with nodal values U^j corresponding to time t^j. The flow front position at time t^j is denoted as h^j.

The implementation performs the solution of the filtration and flow problems as well as property updating as shown in Fig. 2. The solution of the filtration problem is performed first at each increment via the discretised forms of Eqs.3 and 4. Using a forward scheme Eq.4 yields

$$\sigma_i^j = \sigma_i^{j-1} + \left(t^j - t^{j-1}\right)\left(k_0 U^{j-1} C_i^{j-1} - k_r U^{j-1} \sigma_i^{j-1}\right), \quad i = 0...j-1 \tag{15}$$

which accompanied by the boundary condition at the flow front ($\sigma_i^j = 0$) allows the explicit calculation of the retained concentration profile at time t^{j+1} based on the solution for the previous increment.

The finite difference form of Eq. 3 follows a backward time-forward space scheme

$$C_{i+1}^{j} = C_{i}^{j} + \frac{\Delta x}{U^{j-1}}\left[-\varepsilon_{i}^{j-1}\frac{C_{i}^{j} - C_{i}^{j-1}}{t^{j} - t^{j-1}} - \frac{\sigma_{i}^{j} - \sigma_{i}^{j-1}}{t^{j} - t^{j-1}}\right], \quad i = 0...j-1 \tag{16}$$

which accompanied by the condition of prescribed concentration at the inlet ($C_{0}^{j} = 0$) allows the explicit calculation of the suspended concentration at nodal points, using the suspended concentration solution for the previous increment and the retained concentration solution for the current increment. The calculation of the retained and suspended concentration allows the updating of material properties via Eqs.12-14, which enables the solution of the flow problem to be made taking into account the non-linearities due to filtration. The finite difference formulation of the flow problem differs depending on the type of boundary condition at the inlet (Eq.6). In the case of flow control (Eq.6.b) the fluid velocity is known a priori and Eq.2 can be solved explicitly using a trapezoidal scheme

$$P_{i-1}^{j} = P_{i}^{j} + V_{0}\left(\varepsilon_{i-1}^{j}\frac{\eta_{i-1}^{j}}{K_{i-1}^{j}} + \varepsilon_{i}^{j}\frac{\eta_{i}^{j}}{K_{i}^{j}}\right)\frac{\Delta x}{2}, \quad i = 0...j-1 \tag{17}$$

subject to the boundary condition of prescribed pressure at the flow front ($P_{i}^{j} = P_{\infty}$).

In the case of pressure control (Eq.6.a) a centered approximation of Eqs.1 and 2 yields

$$P_{i+1}\left(\frac{K_{i+1}}{\eta_{i+1}} + \frac{K_{i}}{\eta_{i}}\right) - P_{i}\left(\frac{K_{i+1}}{\eta_{i+1}} + 2\frac{K_{i}}{\eta_{i}} + \frac{K_{i-1}}{\eta_{i-1}}\right) + P_{i-1}\left(\frac{K_{i}}{\eta_{i}} + \frac{K_{i-1}}{\eta_{i-1}}\right) = 0, \quad i = 0...j-1 \tag{18}$$

which accompanied by the outlet condition and the inlet pressure boundary condition ($P_0^j = P_o$) form a system of equations that is solved to compute the pressure profile approximation.

The implementation of the flow solution follows the generic boundary condition expressed by Eq.6.c. When the code starts flow control is enabled and at the end of each increment the pressure at the inlet is compared with the pressure constraint P_o. If the inlet pressure is greater than P_o pressure control is enabled. The monotonous increase of pressure at the inlet ensures that once pressure control is enabled the status of the type of solution required does not change.

3. Results and discussion

3.1. Convergence and stability of the finite difference model

Successful simulation of the non linear flow/filtration fields using finite differences is conditional on the appropriate numerical behaviour of the scheme proposed. The convergence of the scheme is supported by theoretical evidence available for the linear version of the problem as well as empirical evidence that concerns the full non-linear version of the flow and filtration set of differential equations (Eqs.1-6 and 12-14).

The linear version of the filtration problem, where properties are constant and re-suspension is considered negligible ($k_r=0$), can be addressed by applying the Von Neumann stability analysis on the combination of Eqs.15-16. Taking into account the relation between time step and velocity yields

$$C_{i+1}^j = C_i^{j-1} - k_o \Delta x C_i^{j-1} \tag{19}$$

which corresponds to the following error growth factor

$$g(l) = \frac{1 - k_o \Delta x}{\exp(I\, l \Delta x)} \tag{20}$$

with $\sqrt{I} = -1$. Stability is ensured if $|g(l)|^2 \leq 1$ which holds unconditionally. The stability of the retained concentration solution for the linear case follows, as the integration implied by Eq.15 converges when the term $k_o UC$ is bounded and continuous. The linear versions of Eqs.17-18 result in linear systems of equations with a bounded inverse matrix and thus are unconditionally stable.

The consistency of the finite difference scheme in the linear case is tested via a comparison with the analytical solution of the flow/filtration problem (Eqs.7-11). The input parameters utilised, which correspond to in-plane filling of an epoxy/0.25 wt.% CNT carbon fibre composite, are listed in Table 1 (column Linear case). The inlet boundary condition of the flow problem is flow control under a pressure constraint (Eq.6.c). Finite difference simulations were carried out using a grid with 4 to 97 nodes. A comparison between the finite difference solution and the analytical model is illustrated in Fig. 3. The simulation converges to the analytical solution as the relative error in the computation of pressure, flow front position, and retained and suspended concentrations is about 5% for a grid with more than 50 nodes and 2% for a grid size with more than 100 nodes (Fig. 3(a)). The evolution of the flow front position predicted by the finite difference solution converges to the analytical solution as the grid is refined (Fig. 3(b)), with the solutions being practically indistinguishable for a mesh with more than 30 nodes. The distributions of field variables (pressure, particle concentration) become virtually identical to the analytical solution as the grid is refined; the results in Figs. 3(c) and 3(d) showing the distribution of pressure and retained particles at a flow front position of 0.2 m are typical of all filling times. The distribution of suspended particles, which is not shown in this figure, follows an exponential dependence on position and shows similar convergence behaviour.

Further evidence of the convergence properties of the finite difference scheme can be obtained by a mesh stability analysis for the case of non-linear properties. The model inputs for this investigation are listed in Table 1 (column Non-linear case 1) and the results are illustrated in Fig. 4. The finite difference solution of a very fine mesh (0.2 m long grid with 129 nodes) is used as a reference for the calculation of the error. The average relative error is below 5% for a grid with more than 40 nodes and decreases to values below 2% at a grid with about 65 nodes. The flow front position converges to the finer mesh values for a grid with more than 20 nodes (Fig. 4(b)). Equivalent stability is observed for the pressure distribution and concentrations; the results for pressure and retained concentration at a flow front position of 10 cm (Fig. 4(c) and 4(d)) are characteristic of the whole solution.

The analysis presented here demonstrates the validity of the finite difference model solution as the linear case can be shown to be stable and consistent with the analytical solution. Furthermore, the non-linear version of the finite difference model is stable with mesh refinement. Thus, the numerical implementation can be considered appropriate. Future experimental validation will allow testing of the validity of the material laws used.

3.2. Range of applicability of the analytical model

The analytical model is preferable in the context of process design mainly due to the computational efficiency, when iterative use is necessary, as well as the relative simplicity of its input. An evaluation of the range and extent of its validity in approximating a non-linear situation is valuable deciding whether its usage is adequate in a certain design situations. Two process parameters were identified as the most appropriate set for evaluating the effect of non-linearity; namely the filtration constant

(k_o), which was varied between 0.01 and 10 m^{-1}, and the length of the filling domain (L), which was varied between 1 mm and 10 m. The study was carried for two different nanoparticle loadings (0.25 and 0.625 wt.%). Other factors influencing non-linearity such as intrinsic viscosity as well as porosity and permeability variations could be included in such a study. However, these are limited in a relatively narrow range for realistic systems and their variations can be considered of secondary importance.

Simulations were carried out using the inputs listed in Table 1 (column Non-linear case 2) and the average relative difference between the results of the analytical simulation and the non-linear finite difference solution was calculated. Fig. 5 summarises the error distributions over the filtration constant-length space for the two loading levels investigated. The error of the analytical solution increases as both the filtration constant and length increase, showing a stronger effect of non-linearity for higher values of these parameters as expected. The effect of loading is also positive on the error as it can be seen by comparing Figs. 5 (a)-(c) with Figs. 5 (d)-(f). For the low loading (Figs. 5 (a)-(c)) the error of the analytical solution is limited below approximately 3 % for lengths up to 1 cm. This result is relevant for through thickness infusion and shows that the analytical approximation can be used in this scenario. The sensitivity to the filtration constant is also limited in this range of lengths with the error remaining practically constant up to filtration constant levels over 100 $\%.m^{-1}$. As the length increases the sensitivity to the filtration constant increases, with error approaching 10% in the 10-50 $\%.m^{-1}$ filtration constant range (Figs. 5 (a)-(c)) for lengths corresponding to in-plane filling (~1 m). Thus, the applicability of the analytical solution in in-plane processes is limited to the cases of low filtration constants. The errors in total concentration (Fig. 5 (c)) tend to be lower than for pressure and flow front

position as a result of the significant steady state component in the solution for suspended concentration. The results for high loading (0.625 wt.%) follow the same trends with an overall stronger effect of non-linearity. Thus, the low error area is limited to lengths below a few millimetres – a value which is still relevant to through thickness infusion. Similarly, the transition to levels of error over 10 % for lengths relevant to in-plane processes (~1 m) occurs in the 1-10 $\%.m^{-1}$ filtration constant range. Overall, these results indicate that the analytical solution is useful in through thickness infusion and limited to only very low filtration constants in in-plane infiltration of hybrid composites. It should be noted that the flow solution differences are governed by variations in resin viscosity. For the cases investigated here, significant errors (over 5%) arise once the difference in viscosity between the linear and the non-linear model reach 65 mPas. Use of the finite difference model is appropriate in conditions outside this envelope.

4. Conclusions

The analytical approximation and the non-linear finite difference model developed here offer a complementary range of solutions for the simulation of flow and filtration in liquid moulding of nanoparticle loaded resins. The analytical approximation can be applied to processes involving short filling lengths, i.e. through thickness infusion. The non-linear numerical approximation is appropriate for processes involving infiltration lengths in the meter range, e.g. resin transfer moulding.

The models have been verified in terms of consistency and, for the numerical case, convergence. Future experimental validation will allow evaluation of the material models selected here as well as the basic physical laws used for the representation of the flow and filtration phenomena. Extensions to different material models, which can incorporate different retention or suspension kinetics, different viscosity and

permeability dependence on loading as well shear rate dependent rheological behaviour of the suspensions, can be implemented as part of the current numerical formulation, whilst development of the necessary characterisation and validation datasets is required for application of the models in industrial situations.

The models can find direct application to the expanding field of processing of hybrid composites. Process feasibility investigations are possible using both the analytical and the numerical solutions. The analytical model lends itself to process design due to its computational efficiency and simplicity in input parameters. Furthermore, these models enable process design of graded nanocomposites to be made. The capability to predict the distribution of concentration of nanoparticles will lead to the development of processes producing hybrid composites with strategically selected nanoparticles distribution, maximising both performance and efficiency of the reinforcement.

5. References

[1] Fiedler B, Gojny FH, Wichmann MHG, Nolte MCM, Schulte K. Fundamental aspects of nano-reinforced composites. Compos Sci Technol. 2006;66(16):3115-3125.

[2] Thostenson ET, Ren Z, Chou T-W. Advances in the science and technology of carbon nanotubes and their composites: a review. Compos Sci Technol. 2001;61(13):1899-1912.

[3] Herzig JP, Leclerc DM, Goff PL. Flow of suspensions through porous media - Application to deep filtration. Ind Eng Chem. 1970;62(5):8-35.

[4] Maroudas A, Eisenklam P. Clarification of suspensions: a study of particle deposition in granular media: Part I - Some observations on particle deposition. Chem Eng Sci. 1965;20(10):867-873.

[5] Sakthivadivel R. Clogging of a granular porous medium by sediment. Report HEL, Berkely: University of California; 1969.

[6] Ryan JN, Elimelech M. Colloid mobilization and transport in groundwater. Colloids Surf, A. 1996;107:1-56.

[7] Geissler S, Wintgens T, Melin T, Vossenkaul K, Kullmann C. Modelling approaches for filtration processes with novel submerged capillary modules in membrane bioreactors for wastewater treatment. Desalin. 2005;178(1-3):125-134.
[8] Shapiro AA, Bedrikovetsky PG, Santos A, Medvedev OO. A stochastic model for filtration of particulate suspensions with incomplete pore plugging. Transp Porous Media. 2007;67(1):135-164.
[9] Elgafy A, Khalid L. Carbon nanoparticle-filled polymer flow in the fabrication of novel fiber composites. Carbon. 2006;44(9):1682-1689.
[10] Elgafy A, Khalid L. Engineering solution in monitoring nanoparticle-fluid flow during nanocomposites processing. J Nanopart Res 2007;9(3):441-454.
[11] Hwang WR, Advani SG, Walsh S. Direct simulations of particle deposition and filtration in dual-scale porous media. Compos Part A. 2011;42(10):1344-1352.
[12] Nordlund M, Fernberg SP, Lundström TS. Particle deposition mechanisms during processing of advanced composite materials. Compos Part A. 2007;38(10):2182-2193.
[13] Destephen JA, Choi KJ. Modelling of filtration processes of fibrous filter media. Sep Technol. 1996;6(1):55-67.
[14] Erdal M, Güçeri S, Danforth SC. Impregnation molding of particle-filled preceramic polymers: Process modeling. J Am Ceram Soc. 1999;82(8):2017-2028.
[15] Lefevre D, Comas-Cardona S, Binetruy C, Krawczak P. Modelling the flow of particle-filled resin through a fibrous preform in liquid composite molding technologies. Compos Part A. 2007;38(10):2154-2163.
[16] Lefevre D, Comas-Cardona S, Binetruy C, Krawczak P. Coupling filtration and flow during liquid composite molding: Experimental investigation and simulation. Compos Sci Technol. 2009;69(13):2127-2134.
[17] Chohra M, Advani SG, Gokce A, Yarlagadda S. Modeling of filtration through multiple layers of dual scale fibrous porous media. Polym Compos. 2006;27(5):570-581.
[18] Steggall-Murphy C, Simacek P, Advani SG, Barthelemy A, Yarlagadda S, Walsh S. A model for particle deposition during impregnation of fibrous porous media. J Porous Media. 2011;14(5):383-394.
[19] Gebart BR. Permeability of unidirectional reinforcements for RTM. J Compos Mater. 1992;26(8):1100-1133.

[20] Advani SG, Sozer EM. Process modeling in composites manufacturing. 2nd ed. New York: CRC Press; 2010.
[21] Krieger IM, Dougherty TJ. A mechanism for non-Newtonian flow in suspensions of rigid spheres. Trans Soc Rheol 1959;3(1):137-152.

Table 1. *Input parameters used in simulations. Column Linear case corresponds to the comparison between linear finite differences and analytical solution in section 3.1; column Non-linear case 1 corresponds to the stability analysis for the non-linear finite differences model in section 3.1;column non-linear case 2 corresponds to the study of limits of validity of the analytical solution in section 3.2.*

Parameters	**Linear case**	**Non-linear case 1**	**Non-linear case 2**
K **[m^2]**	$1.57\ 10^{-11}$	$1.57\ 10^{-11}$	$1.57\ 10^{-11}$
η_o**[Pas]**	-	0.054	0.054
η**[Pas]**	0.211	-	-
ε_o	0.43	0.43	0.43
P_o **[Pa]**	$2.0\ 10^5$	$2\ 10^5$	$2\ 10^5$
P_∞ **[Pa]**	$2.0\ 10^3$	$2\ 10^3$	$2\ 10^3$
V_o**[m/s]**	$7.43\ 10^{-3}$	$7.43\ 10^{-3}$	$7.43\ 10^{-3}$
C_o **[kg/m^3]**	2.78	5.56	2.78, 6.95
ρ_{NP} **[kg/m^3]**	1660	1660	1660
A	-	$6.4\ 10^{-11}$	$6.4\ 10^{-11}$
ϕ_m	-	0.55	0.55
η_I	-	812.6	812.6
k_o**[m^{-1}]**	0.1	0.1	0.01-10
k_r	0	0	0
L**[m]**	0.3	0.2	0.001-10

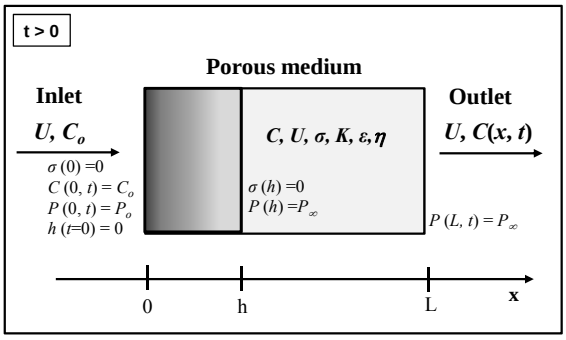

Fig. 1 Schematic of the flow and filtration problem

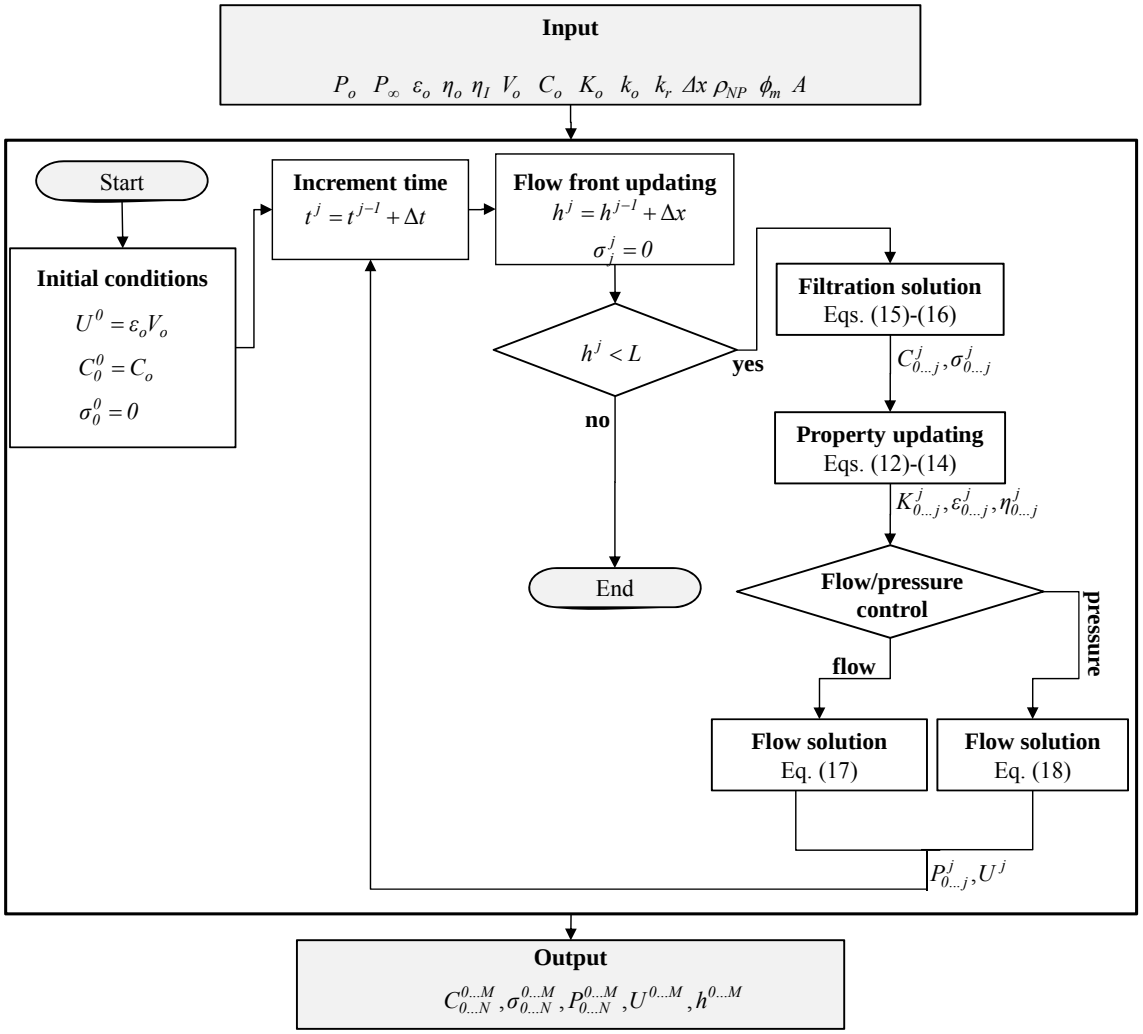

Fig. 2 *Flow chart of the flow and filtration FD model implementation.*

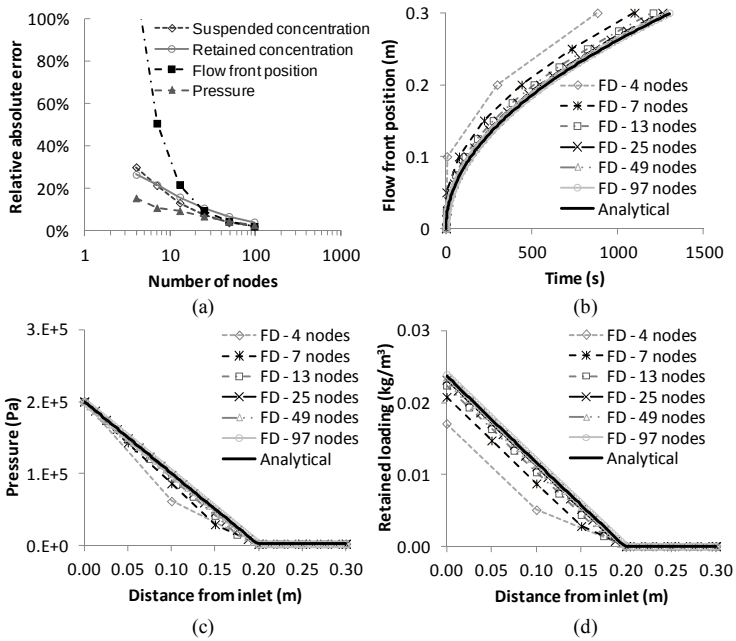

Fig. 3 *Consistency and convergence of the finite difference solution based on a comparison with the analytical solution in the linear case: (a) average relative error against the analytical solution; (b) flow front position evolution; (c) pressure distribution for flow front at 0.2 m; (d) distribution of retained loading for flow front at 0.2 m. The parameters of the model are listed in Table 1 (Linear case).*

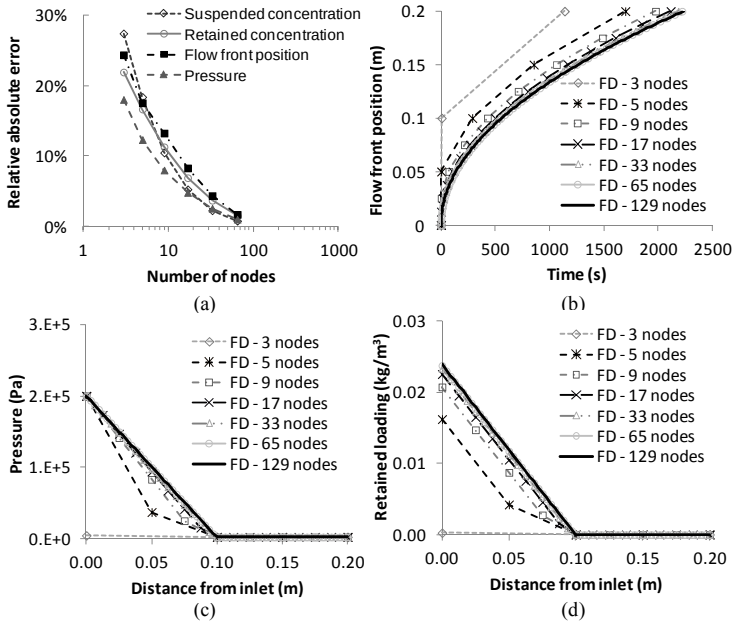

Fig. 4 *Stability of the finite difference solution with respect to mesh refinement: (a) average relative error against the finest mesh (129 nodes in a 0.2 m grid); (b) flow front position evolution; (c) pressure distribution for flow front at 0.1 m; (d) distribution of*

retained loading for flow front at 0.1 m. The parameters of the model are listed in Table 1 (Non-linear case 1).

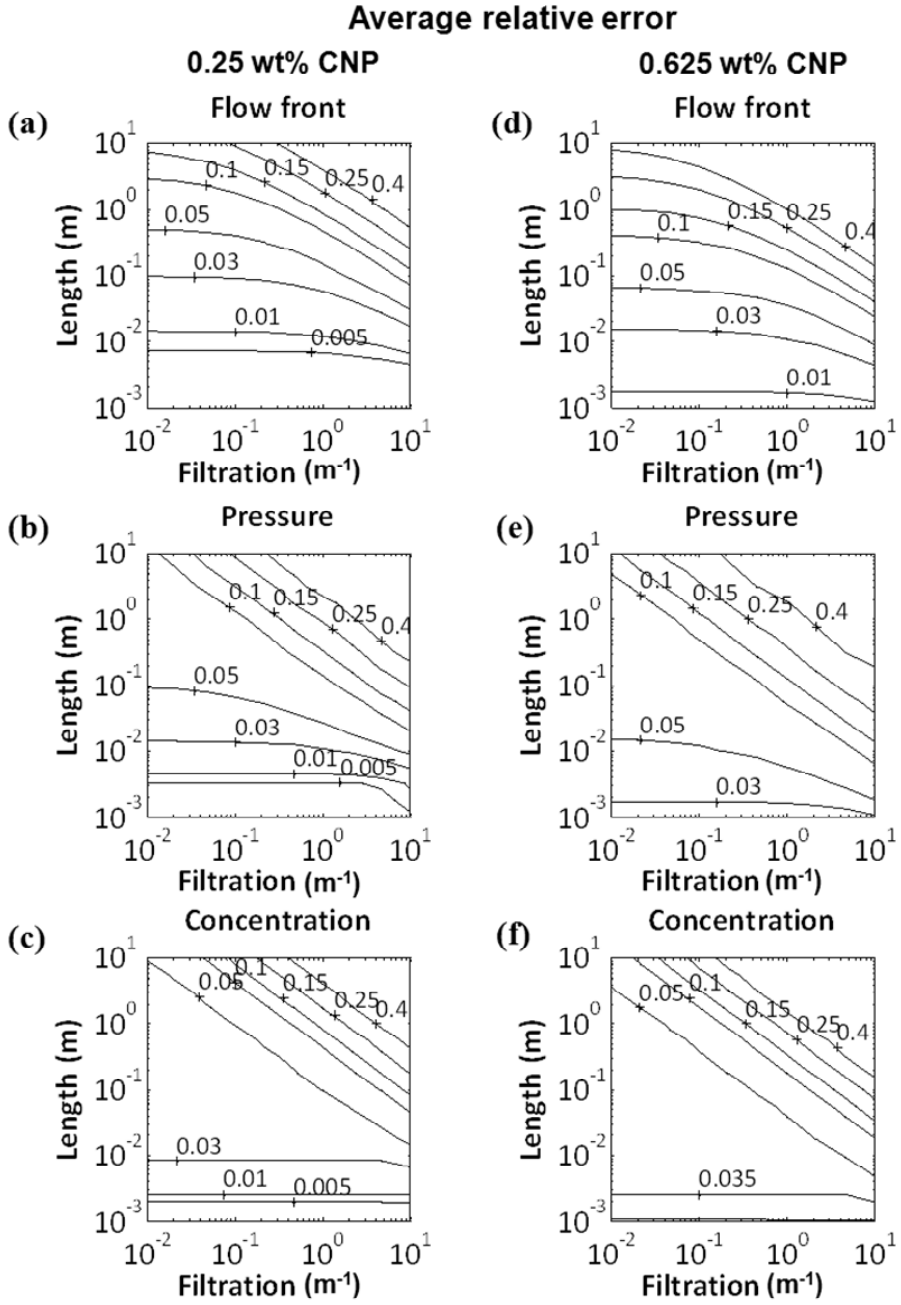

Fig. 5 *Limits of applicability of the linear analytical solution using the non linear finite difference solution as a benchmark: (a)-(c) average relative error in flow front position, pressure and total concentration for low nanoparticle content (0.25 wt.%); (d)-(f) average relative error in flow front position, pressure and total concentration for high nanoparticle content (0.625 wt.%); The parameters of the model are listed in Table 1 (Non-linear case 2).*